STUDIA UBB CHEMIA, LXX, 1, 2025 (p. 35-46)
(RECOMMENDED CITATION)
DOI:10.24193/subbchem.2025.1.03

SYNTHESIS OF N-DOPED CARBON MATERIALS WITH ULTRA-MICROPOROUS BY ACTIVATIVE RUBIDIUM CHLORIDE

Baocheng WU[a,b], Ye XING[a], Yande CAO[a,c], Haichao LI[a,*]

ABSTRACT. Activated carbon from quinoa straw, an agricultural waste, was prepared by chemical activation using a novel activator, rubidium chloride. The effects of time, temperature and amount of activator on the yield and adsorption properties of quinoa straw activated carbon were also investigated. The results showed that the optimal activation process for quinoa straw activated carbon was: activation temperature 700 ℃, activation time 2 h, and RbCl-QS ratio 1:1. The quinoa straw activated carbon prepared under this process had a yield of 27.18%, an iodine adsorption value of 828.11 mg g^{-1}, a total pore volume of 0.303 cm^3 g^{-1}, a major pore size of 0.58 nm, and a specific surface area of 635.59 m^2 g^{-1}. At room temperature and pressure, the H_2 desorption can reach 3.92 cm^3 g^{-1}. quinoa straw activated carbon prepared using RbCl as activator has excellent adsorption and hydrogen storage properties.

Keywords: *Ultra-microporous, Activated carbon, Hydrogen adsorption storage, Chenopodium quinoa Willd., rubidium chloride*

INTRODUCTION

Hydrogen energy has significant advantages such as zero carbon, high efficiency, high calorific value, cleanliness and non-pollution. It can be used as an ideal substitute for fossil energy in the future. In recent years, with

[a] *Key Laboratory of Applied Physical Chemistry of Qinghai Province, Qinghai Minzu University, Xining 810007*
[b] *China School of Chemical Engineering and Automation, Qinghai Vocational and Technical University, Xining 810016, China*
[c] *Asia Silicon (Qinghai) Co., Ltd, Xining 810007, China*
[*] *Corresponding author: lihaichao@vip.163.com*

the continuous research on hydrogen storage materials. Hydrogen storage materials have been widely used in the fields of transportation, industry and construction [1]. However, hydrogen being a chemically active gas, hydrogen storage technology is considered to be the key bottleneck limiting the large-scale commercial application of hydrogen energy [2]. Hydrogen storage materials have been widely studied, including metal complex hydride hydrogen storage materials, solid state hydrogen storage materials, and organic liquid hydrogen storage materials. However, metal complex hydride hydrogen storage materials have low storage pressure but poor cyclic stability [3]; Solid-state hydrogen storage materials are safe, do not require high pressure, and are easy to transport, but have harsh release conditions [4]; Organic liquid hydrogen storage materials have high hydrogen storage density, high safety, convenient storage and transportation, expensive cost and harsh reaction conditions limit their development [5]. In summary it is necessary to develop a new hydrogen storage material.

Quinoa is native to the middle and high altitude mountains of the Andes in South America. It is now widely planted in China's Qinghai, Gansu, Tibet and other provinces. Due to its high cold tolerance, high yield and short growth cycle. It has become one of the few specialty crops that can be grown in the Tibetan Plateau region [6,7]. The massive cultivation of quinoa has made the problem of quinoa straw treatment progressively more acute. Unsilaged quinoa straw cannot be eaten by cattle. Leaving it in the field will interfere with the following year's cultivation. In the past, burning was used in most of the treatments, which can pollute the environment. It is also a serious waste of resources [8]. Like most plant straws, quinoa straw's main components are lignin, cellulose and hemicellulose. In a previous study, activated carbon (AC) prepared from straw after activation had better adsorption and energy storage properties [9]. Most of the traditional activators used in the preparation of AC are zinc chloride, phosphoric acid and potassium hydroxide. Most of the activators are not recyclable and need to be pH-neutralized after activation, and even produce toxic gases [10]. The selection of activators has hindered the development of AC materials. The Tibetan Plateau region is rich in salt lakes. Chloride-type salts usually have high melting points [11,12]. It is considered as an activator for the preparation of AC materials, which is of great significance for the application of salt resources in Qinghai Province.

In this experiment QS was used as a carbon source and RbCl as an activator. The activation of quinoa straw by the chemical activation method allowed the complete recovery of RbCl at the end of the experiment.

RESULTS AND DISCUSSION

The fixed activation temperature was 700°C and the activation RbCl-QS ratio was 1:1. The effect of activation time (0-3 h) on the yield of QSAC and the adsorption performance of iodine value was investigated. As can be seen from Figure 1(a), the iodine adsorption value of QSAC increases with the increase of activation time from 0 to 2 h. The yield (27.18%), iodine adsorption value (765.35 mg g^{-1}) of QSAC at 2h was greater than the values obtained at other activation times. At 3 h, the yield and iodine adsorption value were significantly reduced compared with that at 2 h. Therefore, 2.0 h was selected as the optimal time.

The fixed activation time was 2 h, and the activation RbCl-QS ratio was 1:1. To investigate the effect of activation temperature (500~800 °C) on the yield of QSAC and iodine adsorption value. From Figure 1(b), it can be seen that the QSAC yield decreased from 33.81% to 17.37% with the increase of activation temperature. The iodine adsorption value increased continuously, and at 700 °C the iodine adsorption value (794.21mg g^{-1}). The iodine adsorption value decreased when the temperature reached 800 °C, when the yield (17.37%) and iodine adsorption value (574.43 mg g-1) were the lowest. Therefore, 700 °C is selected as the optimal temperature.

The activation temperature was fixed at 700 °C and the activation time was 2 h. To investigate the effect of activated RbCl-QS ratio on QSAC yield as well as iodine adsorption value. From Figure 1(c), it can be seen that at a RbCl-QS ratio of 0.5:1 (18.33%), the QSAC yield was the lowest compared to 1:1 (27.09%) and 1:2 (29.46%). At RbCl-QS ratio 2:1, there was no remarkable increase in QSAC yield and iodine adsorption values compared to 1:1. The optimal RbCl-QS ratio was chosen to be 1:1 from the economic point of view. Higher iodine adsorption values of activated carbon will result in better performance. In summary, an activation time of 2 h, an activation temperature of 700 °C and a RbCl-QS ratio of 1:1 was chosen as the characterization samples in the following experiments.

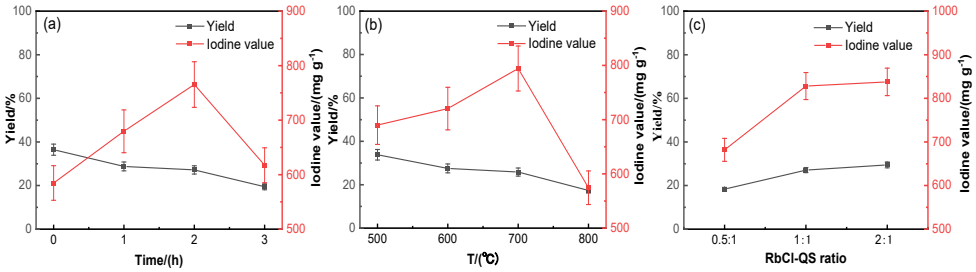

Figure 1. Effect of activation parameters on QSAC yield and adsorption performance

STRUCTURAL CHARACTERISTICS

The original image of RbCl is shown in Figure 2(a) reveal boulder like particles of RbCl with diameters of about 5 – 15 μm. The carbonised samples do not evidence such large particles indicating that the RbCl remains after carbonisation should be nanostructured, such a fact can be proved by the XRD patterns applying the Scherrer formula on the RbCl peaks. The surface of uncarbonised quinoa straw as shown in Figure 2(b) is smooth, compact and fewer pores. As shown in Figure 2(c), without adding any activator, the surface of quinoa straw carbon (QSC) was rough and the plant tissues were severely damaged. As shown in Figure 2(d-f), the pores on the surface of carbonised QS increased significantly. As the RbCl-QS ratio gradually increased, the vascular bundles and basic tissues of QSAC were more intact, the surface was smoother and less porous, and most of the vascular bundles were hardly broken and collapsed.

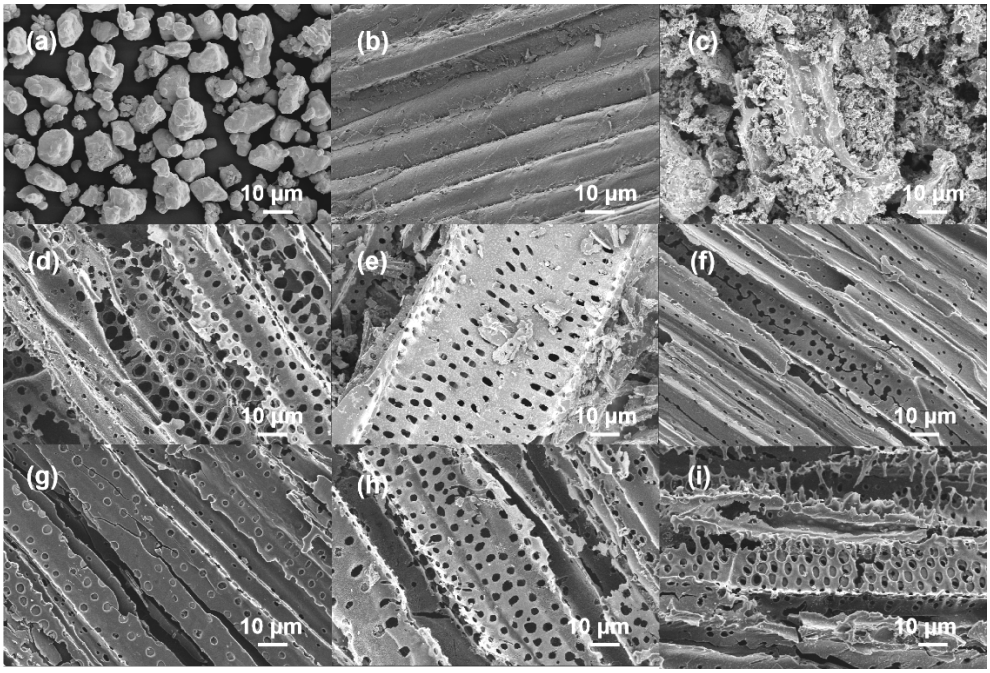

Figure 2. SEM image of the samples. (a) RbCl; (b) Quinoa Straw; (c) QSC700; (d) RbCl-QS ratio 0.5:1 QSAC700; (e) RbCl-QS ratio 1:1 QSAC700; (f) RbCl-QS ratio 2:1 QSAC700; (g) RbCl-QS ratio 1:1 QSAC500; (h) RbCl-QS ratio 1:1 QSAC600; (i) RbCl-QS ratio 1:1 QSAC800

As shown in Figure 2 (g-i), the number of pores increases significantly with increasing carbonation temperature. Compared to QSC, the surface of QSAC maintains the basic characteristics of the plant's microstructure. At higher temperatures and less RbCl, part of the microporous structure was damaged, leading to a decrease in the specific surface area of QSAC. The surface of QSAC is smooth and becomes more microporous, which has a larger specific surface area as well as better hydrogen adsorption capacity compared to QSC. It may be due to the addition of RbCl as an activator, which acts as a flame retardant and slows down the release of gaseous small molecules such as aromatic hydrocarbons, allowing the microstructure of the plant to be preserved. At the same time, during the gradual increase in temperature, small molecules such as aromatic hydrocarbons are slowly released, creating a large number of ultra-micropores [13].

As shown in Figure 3(a), the AC adsorption-desorption isotherm conforms to type I according to the IUPAC New Code-2015 Physical Adsorption Isotherm Classification method, which shows that the QSAC has a very high adsorption value of N_2, as high as 196.13 cm^3 (STP) g^{-1} [14]. The adsorption isotherm has a larger slope in the low relative pressure region, especially in the low-pressure part (P/P_0 < 0.01) of the adsorption. N_2 adsorption tends to equilibrate with increasing relative pressure. This is mainly due to stronger interactions, indicating that QSAC is dominated by micropores. According to the BET method, the total pore volume of QSAC700 was 0.303 cm^3 g^{-1}, an overall distribution concentrated in the range of 0.58-0.73 nm, and a specific surface area of 635.59 m^2 g^{-1}. The results of the nitrogen adsorption-desorption curves are further corroborated from the pore size distribution plot in Figure 3(b). The QSAC700 dominant pore size distribution is at 0.58 nm. According to the IUPAC New Specification-2015 Code it can be determined that QSAC700 is a new type of ultra-microporous carbon material.

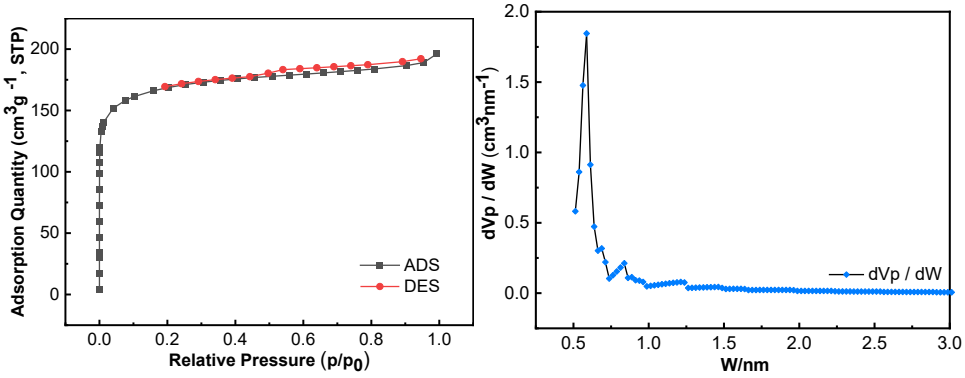

Figure 3. (a) N_2 adsorption-desorption isotherms, (b) Pore size distribution of QSAC700

The grey, blue and green XRD patterns in Figure 4(a) have a less intense and broadened peak at 27.15° which belongs to RbCl according to PDF 89-3623. The QSC700 does not have any peak at 27.15°. The intensity of peak at 27.15° is small in the grey pattern corresponding to less amount of RbCl and it progressively increases for the blue and green patterns due to the increased amount of RbCl. The peak at 27.15° is slightly broadened for all grey, blue and green patterns indicating that RbCl remains in the carbonised samples are nanostructured, that's why they are not visible on the SEM images. Applying Scherrer formula to the mentioned peaks; according to my calculations it results the following diameters for the RbCl nanoparticles: Grey pattern 25 nm, Blue pattern 60 nm, Green pattern 90 nm. Meanwhile, the structural orderliness of QSAC700 was analysed by XRD, as shown in Figure 4(a). It can be seen that all samples had distinct characteristic diffraction spectrum of carbon. The (002) crystal plane and the (100) crystal plane have typical amorphous carbon characteristics at 2θ of about 26° and 43°. The d_{002} graphite layer spacings of QSC and QSAC at different RbCl:QS ratios of 2:1, 1:1, and 0.5:1 were calculated from Bragg's formula to be 0.350 nm, 0.426 nm, 0.354 nm, 0.387 nm, which is larger than the layer spacing of fully non-graphitised carbon (0.344 nm). It can be demonstrated that the prepared QSAC are in the amorphous carbon stage, which can be graphitised by increasing the temperature. As shown in Figure 4(b), the presence of distinct D, G and 2D band in QSAC700 is typical of amorphous carbon. The intensity ratio of the D and G bands (I_D/I_G) has long been considered a key parameter for analyzing graphitization levels [15]. The calculated I_D/I_G ratio of AC700 is 0.9263, which indicates that the prepared QSAC possesses some degree of graphitization [16]. This indicates that the interior of QSAC is transforming from a graphite disordered layer structure to an ordered one, and the microcrystalline defects are gradually reduced. The slightly bulged 2D band near 2700 cm^{-1} also confirms that there are still some defects purely in the graphite layered structure.

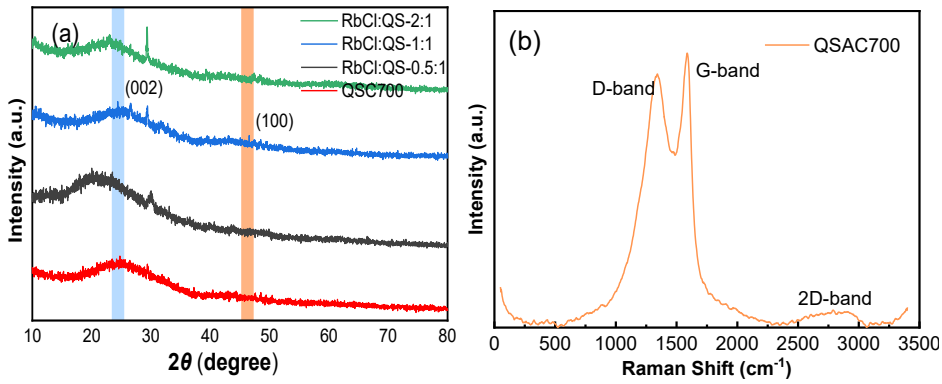

Figure 4. (a) XRD spectra and (b) Raman spectra of the samples

As can be seen in Figure 5, the characteristic peak shapes of QSC and QSAC infrared spectra are almost identical. The peaks around wave number 3 412 cm^{-1} are attributed to the O-H and N-H stretching vibrations; 2 525 cm^{-1} for the methylene and amino stretching vibration peak; The peak with a wave number near 1 808 cm^{-1} is caused by the stretching vibration of the C=C bond of the benzene ring; The peak at 1 464 cm^{-1} is associated with the C-N stretching vibrational mode; The peaks at 1 001 cm^{-1} are those of C-O-C, C-O stretching vibrations and O-H bending vibrations in carboxylates, phenols or alcohols; The peak at 877 cm^{-1} is an out-of-plane deformation vibrational peak of the aromatic ring; The 718 cm^{-1} peak is a bending vibration in the C-C=O plane. It can be seen that the main structure of QSAC consists of multiple aromatic rings. The aromatic ring may also have functional groups such as $-CH_3$, $-CH_2$, -COOH and -OH. The absorption peaks of QSAC at 3 412 cm^{-1} and 1 001 cm^{-1} were significantly broader than those of QSC, suggesting that the QSAC may contain more oxygen-containing functional groups dominated by C-O and O-N bonds. This is due to the increase in the content of highly substituted aromatic rings as a result of the polycondensation of QS by the carbonisation process. Meanwhile, the peak at 1 464 cm^{-1} and 3 412 cm^{-1} can characterise QSAC as a typical nitrogen doped carbon material. Addition of RbCl activator reduces the breakage of chemical bonds connecting the carbon network. It indicates that the prepared QSAC contains sufficient carbon framework and abundant organic functional groups, which in turn makes the QSAC exhibit strong adsorption properties [17].

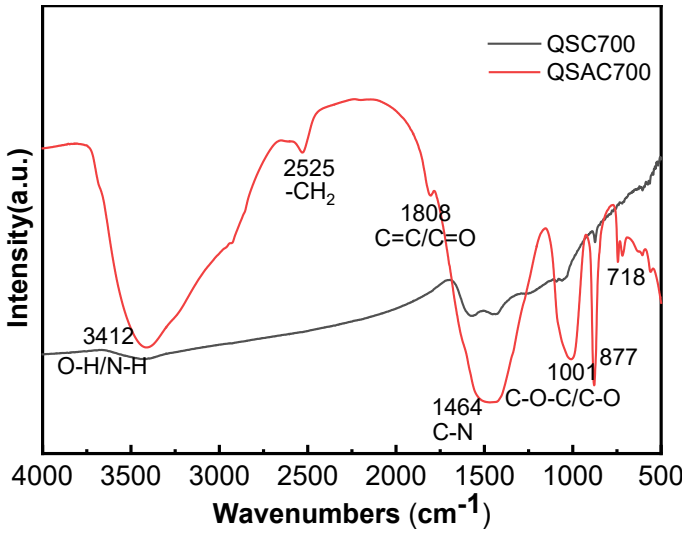

Figure 5. FT-IR spectra of QSC700 and QSAC700

X-ray photoelectron spectroscopy is commonly used to characterise the chemical structure of material surfaces. Figure 6 shows that QSAC700 contains C, N and O elements. From Figure 6 (b) to 6 (d), the C1s spectrum splits into three peaks. It is shown that there are five possible bonding forms of C, namely C=C (284.8 eV), C-O/C=N (286.4 eV) and C-O/C-N (288.4 ev); O1s split into 3 peaks, O-C=O (532.3 eV), C-O (530.8 eV) and C=O (529.5 eV); N1s then splits into 3 peaks, pyridine N (397.2 ev) pyrrole N (398.8 eV) and graphitised N (400.6 eV). Both XPS and FTIR data indicated the presence of O and N in the sample, suggesting that the prepared QSAC700 is N-doped amorphous carbon [18].

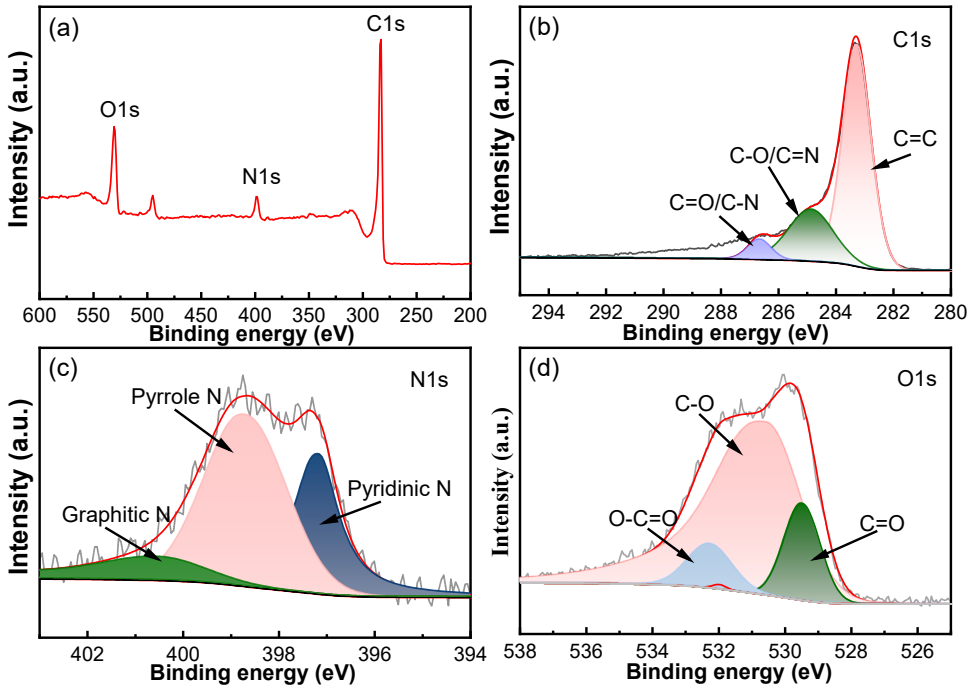

Figure 6. XPS survey (a) and fitted spectra of C1s (b), O1s (c) and N1s (d) of QSAC700

Theoretical calculations and experiments have shown that the physical adsorption of hydrogen on nanomaterials under low-temperature liquid nitrogen conditions depends on the microporous volume and microporous size distribution, especially the microporous volume size is closely related [19]. This is due to the fact that hydrogen molecules are smaller, so their adsorption efficiency is higher on micropores than on mesopores. In general, there is a

good linear relationship between hydrogen storage and microporous pore volume, i.e., the larger the microporous pore volume, the larger the hydrogen storage. S. Schaefer demonstrated that pores with widths ranging from 0.5 to 0.7 nm are best suited for hydrogen storage at 298 K, independent of pressure [20]. Based on this, it is hypothesised that QSAC700 should be a good material for hydrogen storage. The atmospheric pressure hydrogen adsorption and desorption curves for QSAC700 under cryogenic liquid nitrogen conditions are shown in Figure 7. As can be seen from the results in Figure 7, the adsorption capacity of hydrogen reaches 3.92 cm^3 g^{-1} at 298 K and 101.3 KPa, which is higher than the 0.59 wt% reported in literature [20]. It is shown that the QSAC700 microporous structure has excellent hydrogen storage capacity. It is also important to note that QSAC has excellent reversibility as a hydrogen storage material. As the pressure drops, the physically adsorbed hydrogen can be completely and reversibly desorbed without hysteresis loops. With the same specific surface area, the hydrogen storage capacity is higher than that of AC based on rice husk [21], corn kernel [22], bamboo and other raw materials [23], which has a greater application prospect.

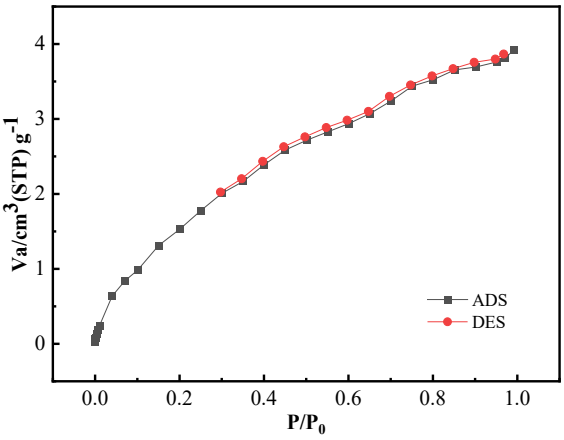

Figure 7. Hydrogen storage capacity of QSAC700

CONCLUSIONS

In the paper, quinoa straw was used as the raw material and RbCl was employed as the activator at 700 °C. QSAC with nitrogen-doped ultra-micropores was prepared by a one-step carbonisation method. The optimal process for the preparation of QSAC was determined by single factor

experiment method as: The activation temperature was 700 ℃, the activation time was 2 h and the RbCl-QS ratio was 1:1. The specific surface area of QSAC reached 635.59 $m^2 g^{-1}$ with a pore volume of 0.303 $cm^3 g^{-1}$ and a dominant pore size of 0.58 nm. Among the carbon materials with the same specific surface area biomass AC, it has a higher percentage of micropores and higher surface nitrogen and oxygen heteroatom content. The adsorption capacity of hydrogen reaches 3.92 $cm^3 g^{-1}$ at room temperature and pressure, which has excellent hydrogen storage capacity. It was demonstrated that RbCl could be used as a novel activator for the activation of quinoa straw for the preparation of N-doped ultra-microporous activated carbon. It provides new ideas for solving the problem of agricultural waste occupying arable land in highland areas and diversified utilization of salt lakes products.

EXPERIMENTAL SECTION

QS was obtained from cultivated land in Haixi Prefecture, Qinghai Province (situated at 37°23′N 97°22′E). Rubidium chloride (RbCl), Iodine (I_2), Potassium iodide (KI), Starch soluble and Sodium thiosulfate ($Na_2S_2O_3$) were purchased from Shanghai Aladdin Biochemical Science and Technology Co., Ltd. and were analytically pure, and the reagent was used directly without special treatment.

QS removed from the plowed fields was washed to remove soil and dried in an oven for 12 hours. After crushing in a pulverizer, it passes through a 200mesh sieve. Using the single factor experiment method, 10 g of QS powder and RbCl were mixed in a crucible in the ratios of 0.5:1, 1:1, and 2:1, respectively, and deionised water was added until it exceeded the QS powder. Due to the non-contact and non-reaction between the solids, RbCl amount is dissolved by the deionised water and fills the pores of quinoa straws and further re-crystallises after heating at 70 C. After removal, the crucible was placed in a muffle furnace. The temperature was increased to 500, 600, 700 and 800 °C at a rate of 10 °C min^{-1} in an air atmosphere. The carbonisation products were obtained by holding the temperature for 1h, 2h, 3h, 4h respectively. The activated samples were then filtered, dried, and ground in a mortar for further study.

SEM: The microstructural features of quinoa straw activated carbon (QSAC) were observed using a Gemini 500 scanning electron microscope from Zeiss, Germany. XRD: Diffraction spectra obtained using a Shimadzu XRD-7000 diffractometer were tested to characterise the microcrystalline structure of QSAC. The XRD investigation was effectuated with Cu kα radiation with a scan rate of 3 (°) /min in the range of 10−80°. Raman: Used for Raman determination

via Thermo Fisher Scientific DxR2XI, USA. The Raman spectrum of QSAC was obtained at an excitation wavelength of 532 nm, and the Raman detection can be used to obtain the degree of graphitization of carbon materials. BET: N2 adsorption/desorption isotherms for QSAC at 77 K were obtained using BELSORPmax from MicrotracBEL Japan, Inc. Specific surface area and micropore volume were based on the Brunauer-Emmett-Teller (BET) method, respectively. Estimation of pore size distribution by Horvath-Kawazoe (HK) model. The adsorption and desorption of H_2 was carried out at 298K. FTIR: The QSAC powder was mixed and ground with KBr powder and then pressed into discs, which were examined Thermo Fisher NICOLET IS20.USA. XPS: Surface functional groups were analysed by X-ray photoelectron spectroscopy with the ESCALAB 250XI model from Thermo Fisher Scientific, USA. Each photoelectron spectral region was scanned several times to obtain a good signal ratio. The C1s peak was set to 284.6 eV and used as an internal standard for the other peaks. The iodine adsorption value is determined according to GB/T 12496.8-2015 “Test methods of wooden activated carbon−Determination of iodine number”.

ACKNOWLEDGMENTS

This work was supported by the Key R&D and Transformation Program of Qinghai (2022-QY-210).

REFERENCES

1. J. W. Ren; N. M. Musyoka; H. W. Langmi; M. Mathe; S. J. Liao; Int. J. Hydrog. Energy, **2017**, 42, 289-311.
2. M. Ayvaz; S. İ. Ayvaz; İ. Aydin; Int. J. Hydrog. Energy, **2018**, 43, 20271-20283.
3. C. G. Michael; S. K. Eustathios; S. M. Sofoklis; K. Konstantinos; N. P. Efstratios; Comput. Chem. Eng., **2009**, 33, 1077-1090.
4. A. Kumar; P. Muthukumar; P. Sharma; E. A. Kumar; Sustain. Energy Technol. Assess., **2022**, 52, 102204.
5. P. C. Rao; Y. S. Kim; H. Kim; Y. H. Son; Y. Y. Choi; K. Na; M. Y. Yoon; ACS Sustainable Chem. Eng., **2023**, 11, 12656-12666.
6. Y. M. Tang; Y. Z. Liu; Y. H. Zhang; Y. N. Cao; P. P. Song; L. M. Hou; L. X. Peng; Food Sci. Nutr., **2024**, 1-13.
7. N. Wang; F. X. Wang; C. Shock; F. B. Fritschi; L. Gao; Z. J. Huang; J. Y. Zhao; Agric. For Meteorol., **2022**, 323, 109084.
8. X. L. Zhao; F. Wang; Y. Fang; D. W. Zhou; S. P. Wang; D. Q. Wu; L. X. Wang; R. Z. Zhong; BioResources, **2020**, 312, 123512.

9. D. Abril; V. Ferrer; G. Y. Mirabal; B. G. Cabrera; C Segura.; A. Marican; A. Pereira; E. F. Durán-Lara; O. Valdés; Materials, **2022**, 15, 4898.
10. C. L. Zhang; H. C. Li; Z. Z. Lin; B. X. Du; X. P. Zhang; Carbon Trends, **2024**, 14, 100322.
11. R. S. DeFever; H. M. Wang; Y. Zhang; E. J. Maginn; J. Chem. Phys., **2020**, 153, 011101.
12. E. Çetingürbüz; A. Turkyilmaz; Ind. Crops Prod., **2023**, 203, 117171.
13. S. Hao; Q. Zhang; Y. Shi; Q. Guo; P. Li; J. Huang; Biomass Conv. Bioref., **2024**, 14, 9581–9594.
14. S. Lee; M. E. Lee; M. Y. Song; S. Y. Cho; Y. S. Yun; H. Jin; Carbon Letters, **2016**, 20, 32-38.
15. D. Guo; Y. Fu; F. Bu; H. Liang; L. Duan; Z. Zhao; C. Wang; A. M. ElToni; W. Li; D. Zhao; Small Methods, **2021**, 5, 2001137.
16. C. Zhou; S. Geng; X. W. Xu; T. H. Wang; L. Q. Zhang; X. J. Tian; F. Yang; H. T. Yang; Y. F. Li; Carbon, **2016**, 108 234-241.
17. Y. Gao; Q. Yue; B. Gao; Y. Sun; W. Wang; Q. Li; Y. Wang; Chem. Eng. J., **2013**, 217 345-353.
18. B. X. Du; H. C. Li; C. L. Zhang; Q. S. Ji; Heliyon, **2024**, 10, e27585.
19. W. Zhao; V. Fierro; N. Fera'ndez-huerta; M. T. Izquierdo; A. Celzard; Int. J. Hydrog. Energy, **2012**, 37, 14278-14284.
20. S. Schaefer; V. Fierro; M. T. Izquierdo; A. Celzard, Int. J. Hydrog. Energy, **2016**, 41, 12146-12156.
21. B. K. Kızılduman; Y. Turhan; M. Doğan; Adv. Powder Technol., **2021**, 32, 4222-4234.
22. T. T. Qin; M. K. Song; K. K. Jiang; J. W. Zhou; W. Zhuang; Y. Chen; D. Liu; X. C. Chen; H. J. Ying; J. L. Wu; RSC Adv., **2017**, 7, 37112-37121.
23. H. S. Jang; J. Y. Mun; W. G. Hong; S. M. Lee; J. W. Jeon; C. Y. Lee; H. J. Kim; B. H. Kim; Int. J. Hydrog. Energy, **2020**, 45, 10516-10522.